This manuscript was accepted and published by ***Energy & Fuels***, a journal of the American Chemical Society.

Publication data of the final, corrected work:

Várhegyi, G.; Szabó, P.; Antal, M. J., Jr.: Kinetics of charcoal devolatilization. *Energy Fuels* **2002**, *16*, 724-731. *doi:* 10.1021/ef010227v

Kinetics of Charcoal Devolatilization.

Gábor Várhegyi[*] and Piroska Szabó[+]

Research Laboratory of Materials and Environmental Chemistry, Chemical Research Center, Hungarian Academy Sciences, P.O. Box 17, Budapest 1525, Hungary

Michael Jerry Antal, Jr.

Hawaii Natural Energy Institute, University of Hawaii at Manoa, Honolulu, Hawaii 96822

Keywords: Charcoal, Carbon, Biomass, Kinetics, Distributed activation energy models, Thermogravimetry – Mass spectrometry.

[*] To whom correspondence should be addressed.
Email: varhegyi.gabor@t-online.hu or gvarhegyi@gmail.com

[+] Present address: COWI Hungary Ltd, Bihary J. u. 20, Budapest 1055, Hungary.

Abstract

The devolatilization kinetics of a biomass charcoal was studied by thermogravimetry - mass spectrometry. The overall mass loss rate (DTG curve) and the mass spectrometric intensities of ions H_2^+, CH_3^+, $C_2H_2^+$, $C_2H_3^+$ and $C_2H_5^+$ were evaluated. The distributed activation energy model (DAEM) was employed, since it can mathematically represent the physical and chemical inhomogeneity of the charcoal. Some of the evaluated experimental curves consisted of 2 - 4 overlapping partial peaks. In those cases parallel reactions were assumed, and each reaction was described by a DAEM. The unknown parameters were determined by a simultaneous least squares evaluation of a series of experiments. Parameters were identified that enabled the model to describe equally well the non-isothermal experiments and the experiments containing isothermal sections. Kinetic information was obtained on the drying and the evaporation of the organics trapped on the surface of the samples; the decomposition of the side groups with low thermal stability; the splitting-off of the more resistant side groups and the formation of the aromatic rings; and the elimination of heteroaromatic oxygen followed by the formation of polyaromatic structures during carbonization.

Introduction

Biomass is a plentiful, renewable resource that can be converted to higher-value gaseous fuels (e.g. hydrogen), liquid fuels (e.g. ethanol), or solid fuels (e.g. charcoal). Recent improvements in the technology for charcoal production have increased its efficiency to such an extent that charcoal yields now approach or equal the theoretical limit.[1-3] Consequently, there is renewed interest in the use of charcoal as a fuel that can be easily stored and transported. High value carbon products (e.g. activated carbon, electrode carbon, etc.) can also be produced from charcoal.

Most industrial processes that utilize charcoal involve a devolatilization step. For example, devolatilization occurs when charcoal is used as a metal reductant. Devolatilization is also an important aspect of charcoal combustion. During devolatilization, the physical and chemical properties of charcoal undergo extraordinary changes that are not well understood. For example, the electrical resistivity of charcoal decreases by six orders of magnitude when charcoal is heated (devolatilized) in an inert environment to 900 ºC.[4] This astronomical change in resistivity creates the opportunity for carbonized charcoal to serve as a fuel in a fuel cell.[5] In light of these facts, one would expect there to be a considerable literature on the chemistry of charcoal devolatilization. Unfortunately, this is not the case. For example, we are unaware of any studies of kinetics of charcoal devolatilization. In light of the underlying importance of charcoal devolatilization to a surprisingly broad range of industrial processes, we undertook this work to gain a deeper insight into the kinetics of charcoal devolatilization.

Devolatilization involves the formation and loss of gaseous species from the parent charcoal. Biomass charcoals are inhomogeneous materials; hence a given species may arise from physically or chemically different sites. In this work we shall deal with these problems. At present, the distributed activation energy model (DAEM) is the best way to represent mathematically the physical and chemical inhomogeneity of a substance. The history and development of this model is well treated in a recent review.[6] Anthony and Howard[7] described coal pyrolysis by assuming a Gaussian distribution of activation energies. Their approach became popular, leading to a substantial number of publications in the areas of coal and biomass pyrolysis, petroleum formation, and natural gas formation.[6] Solomon *et al.* used the DAEM to provide a striking description of the complexity of coal devolatilization.[8] They emphasized that sometimes more than one reaction produced the same species. Accordingly, they combined two or three parallel reactions, and described each of them by a DAEM. Nonisothermal experiments with constant heating rates of 3, 30 and 100°C/min were employed to determine the kinetic parameters. When there were multiple sources for a given species and the sources had overlapping peaks, the determination of parameters was not unique and some simplifying rules had to be assumed. Among others, the preexponential factor for a given species pool was assumed independent of the rank of the coals. Agarwal[9] and Heidenreich et al.[10] followed this approach in their description of the overlapping curves of CH_4 evolved during coal pyrolysis. Agarwal et al.[11] also determined the DAEM kinetics of the evolution of several C_xH_y compounds during coal pyrolysis, assuming

a common log A = 13.22. They carefully compared their results with those of earlier investigations. Recently Lázaro et al.[12] employed a single reaction model with a distributed activation energy to describe the formation of various volatiles from lignin. In their work, A was fixed to 1.67×10^{-13} s^{-1}. The assumptions and evaluation techniques used by these authors resulted in considerably differing parameters for the isothermal and non-isothermal experiments. Several papers have dealt with the numerical integration involved in the DAEM. Recently Donskoi and McElwain[13] proposed the application of a modified Gauss-Hermite quadrature for this purpose.

Experimental.

Sample preparation. A pressure vessel with an internal volume of 7.2 L and various external and internal heaters was used as a semi-batch chemical reactor to produce charcoal for this research.[1] The reactor is capable of converting as much as 5 kg of lignocellulosic materials into high-yield charcoal at elevated pressures (typically 1 MPa) and temperatures (below 400°C). Initially, the biomass is loaded into a canister that is subsequently loaded into the (cold) pressure vessel. After heating and subsequent cool down, the canister full of charcoal is removed from the reactor. For this work, macademia nutshell charcoal[1,14] taken from the canister was divided into three equal sections (upper, middle, and lower). Each section was mixed (separately) and samples from the top and the bottom sections were analyzed (see Table 1). These samples were ground to <120μm in a centrifugal mill flushed with nitrogen continuously, and analyzed by thermogravimetry (TG), thermogravimetry – mass spectrometry (TG-MS) and infrared spectrometry (FTIR).[14] Although the bottom fraction contained fewer volatiles due to temperature inhomogeneities within the reactor, the top and bottom samples showed many similarities.

Table 1: Ultimate analyses (wt% on a dry basis) of the charcoals[17]

Name	C	H	N	Ash	O by difference
Macadamia 1 Top	72.8	4.5	0.6	0.8	21.3
Macadamia 1 Bottom	75.0	4.2	0.6	1.0	19.2

TG-MS Apparatus. A computerized atmospheric pressure thermobalance - mass spectrometer (TG - MS) system was built from a Perkin Elmer TGS - 2 thermobalance and a Balzers QMG - 511 mass spectrometer.[14-15] Selected peak intensities were recorded as functions of time. The evolved gases were led from the TG furnace to the ion source through a heated capillary. The shape of a given mass spectrometric ion intensity as a function of time or temperature has been shown to be a true representation of the rate of mass loss due to the evolution of the parent gas species.[15] The mass spectrometric intensities of CH_3^+, $C_xH_y^+$ and H_2^+ are given in arbitrary units, since there was no way to calibrate the apparatus for these signals (one cannot mimic the experimental conditions of a TG-MS experiment by introducing calibrating gases into the instruments.) The integrated intensities of the detected H_2^+ and CH_3^+ ions represent roughly 40-50 and 6% of

the total ion intensity integral, respectively. The magnitudes of the integrated $C_2H_2^+$, $C_2H_3^+$ and $C_2H_5^+$ ion intensities are similar; each is roughly 0.5% of the integrated total intensity. The mass spectrometric intensity curves were shown in a previous work.[14]

Experimental Conditions. 10, 20, and 40ºC/min heating rates were employed. Parts of the temperature programs included isothermal sections, as shown in Table 2 and Figure 1. The ambient atmosphere was argon. The samples were evenly distributed on a sample pan of 6 mm diameter. The sample size varied between 3 and 4 mg, resulting in overall mass losses of around 1 mg.

Table 2: Summary of the Experiments

No.	Sample (reactor fraction)	Heating rate (°C/min)	*T* of 0.5 h isothermal section (°C)	*T* of 1 h isothermal section (°C)	Symbol in the figures
1	bottom	10	-	-	o
2	bottom	40	-	-	◊
3	bottom	20	133	376	×
4	top	10	-	-	∇
5	top	20	92	337	Δ
6	top	20	133	376	ρ

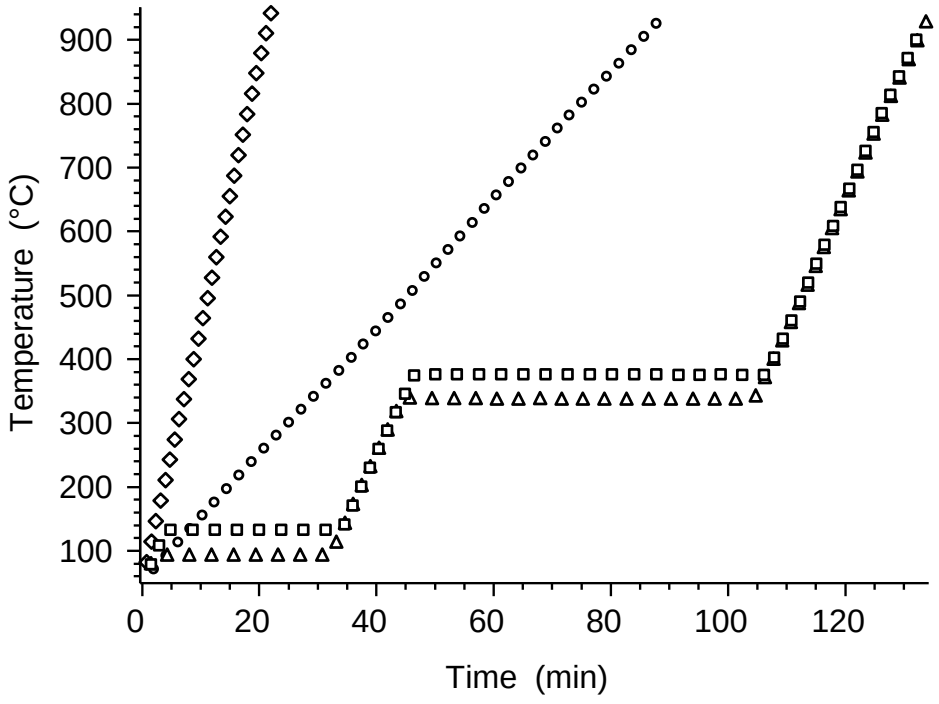

Figure 1: Temperature programs employed in the work. (See Table 2 for details.)

Calculations.

Model. A mass spectrometric ion intensity curve or a DTG curve can be the result of several parallel reactions. Each reaction has its own kinetic equation. Let us denote the unreacted fraction of material represented by the *j*th kinetic equation as x_j. The following boundary conditions apply to functions $x_j(t)$:

$$x_j(0) = 1 \text{ and } x_j(\infty) = 0. \qquad (1)$$

$dx/dt \le 0$ for devolatilization reactions. A mass spectrometric ion intensity curve or a DTG curve ($-dm/dt$) is assumed to be a linear combination of one or more $-dx_j(t)/dt$ functions. Denoting the simulated counterpart of a given experimental curve by $Y^{calc}(t)$, and the coefficients of the linear combination by c_j, we have:

$$Y^{calc}(t) = \sum_{j=1}^{M} - c_j \, dx_j/dt \qquad (2)$$

Here M denotes the number of partial reactions contributing to the given measured quantities. If M=1, there is only one c, which is a proportionality factor between the reaction rate and the observed quantity. When $M > 1$ (i.e. when the observed curve is composed of overlapping partial curves) c_j represents the contribution of the *j*th partial reaction to the measured quantity. Note that the area of a $-dx_j/dt$ curve is 1, as eqn. (1) shows. Accordingly, the c_j coefficients are equal to the areas of the partial peaks. There are separate sets of c_j coefficients for the DTG curve and for each of the mass spectrometric intensities.

Since charcoals are inhomogeneous materials, a given species may arrive from physically or chemically different sites. Accordingly, we shall employ the distributed activation energy model. Let $X_j(t,E)$ denote the solution of a first order kinetic equation at a given E value:

$$-dX_j(t,E)/dt = A_j \exp[-E/RT(t)] \, X_j(t,E) \qquad (3)$$

Here A_j is the preexponential factor and T(t) is the temperature of the reacting particle. $X_j(t,E)$ changes from $X_j(0,E) = 1$ to $X_j(\infty,E) = 0$. Parameters A_j and E determine the rate of this change. Let $D_j(E)$ stand for a normalized distribution function. Then the $x_j(t)$ functions in equations (1) - (2) are defined as

$$x_j(t) = \int_0^{\infty} D_j(E) \, X_j(t,E) \, dE \qquad (4)$$

Several distribution functions have been used in the literature of this type of models[6]; we chose the Gaussian distribution function[7] with parameters $E_{0,j}$ and σ_j:

$$D_j(E) = (2\pi)^{-1/2} \, \sigma_j^{-1} \exp[-(E-E_{0,j})^2/2\sigma_j^2] \qquad (5)$$

The dx_j/dt curves, appearing in formula (2) can be obtained from eqn. (4) as:

$$dx_j(t)/dt = \int_0^{\infty} D_j(E)\, dX_j(t,E)/dt\, dE \qquad (6)$$

Numerical solution. The integration in equations (4) and (6) goes from E=0 to E= ∞. The change of the lower limit of integration enables us to employ generally available mathematical techniques for the integration, without affecting the results, as outlined below:

$$x_j(t) = \int_0^{\infty} D_j(E)\, X_j(t,E)\, dE \cong \int_{-\infty}^{\infty} D_j(E)\, X_j(t,E)\, dE \qquad (7)$$

From a mathematical point of view, a first order kinetic equation possesses a solution at negative E values, too. However, the reaction rate strongly increases as E decreases. As a result, reactions with $E \approx 0$ or $E<0$ terminate much below room temperature at any usual value of A, resulting in $X_j(t,E)=0$ and $dX_j/dt = 0$ in the domain of evaluation. Besides, $D(E) << 1$ at low values of E. Hence approximation (7) can safely be used for the evaluation of thermoanalytical curves.

Introducing a variable

$$\varepsilon_j = (E-E_{0,j}) / \sqrt{2}\, \sigma_j \qquad (8)$$

we can write:

$$x_j(t) \cong (2\pi)^{-1/2}\, \sigma_j^{-1} \int_{-\infty}^{\infty} \exp[-(E-E_{0,j})^2/2\sigma_j^2]\, X_j(t,E)\, dE = \pi^{-1/2} \int_{-\infty}^{\infty} \exp(-\varepsilon_j^2)\, X_j(t, \varepsilon_j)\, d\varepsilon_j \qquad (9)$$

where $X_j(t, \varepsilon_j)$ is $X_j(t,E)$ expressed as a function of ε_j. The above integral can easily be evaluated by a Guass – Hemite quadrature formula[16-17]:

$$x_j(t) \cong \pi^{-1/2} \sum_{i=1}^{N} w_i\, X_j(t,\varepsilon_{ij}) \qquad (10)$$

where w_i and ε_{ij} are (respectively) the weight factors and the abscissas of the quadrature formula. These quantities can be determined by well known Fortran library functions.[17]

In a similar way, we have:

$$dx_j/dt \cong \pi^{-1/2} \int_{-\infty}^{\infty} \exp(-\varepsilon_j^2)\, dX_j(t, \varepsilon_j)/dt\, d\varepsilon_j \cong \pi^{-1/2} \sum_{i=1}^{N} w_i\, dX_j(t,\varepsilon_{ij})/dt \qquad (11)$$

Note that differential eqn. (3) does not have an analytical solution at a general T(t) heating program. Accordingly, the $X_j(t,\varepsilon_{ij})$ and $dX_j(t,\varepsilon_{ij})$ values were obtained by a high-precision numerical solution of eqn. (3) at each ε_{ij} value arising in the calculations.

Recently, Donskoi and McElwain[13] suggested that the energy domain of the integration should be rescaled by a factor of 0.5 – 0.3 to increase the efficiency of the Guass – Hemite quadrature formula. They presented a sophisticated statistical approach for an optimal rescaling. In the present work we employed a rescaling factor of ½ by introducing a variable μ_j:

$$\mu_j = 2\varepsilon_j = 2(E-E_{0,j}) / \sqrt{2}\, \sigma_j \qquad (12)$$

Substituting this variable into eqn. (9) and employing the Gauss - Hermite quadrature for the integration by μ_j, we find:

$$x_j(t) \cong \tfrac{1}{2} \pi^{-1/2} \int_{-\infty}^{\infty} \exp(-0.25\mu_j^2)\, X_j(t, \mu_j)\, d\mu_j \equiv \tfrac{1}{2} \pi^{-1/2} \int_{-\infty}^{\infty} \exp(-\mu_j^2) \exp(0.75\mu_j^2)\, X_j(t, \mu_j)\, d\mu_j \cong$$

$$\cong \tfrac{1}{2} \pi^{-1/2} \sum_{i=1}^{N} w_i \exp(0.75\mu_{ij}^2)\, X_j(t,\mu_{ij}) \qquad (13)$$

Here $X_j(t,\mu_j)$ is $X_j(t,E)$ expressed as a function of μ_j, and w_i and μ_{ij} are the weight factors and abscissas of the Gauss-Hermite quadrature formula. Similarly,

$$dx_j/dt \cong \tfrac{1}{2} \pi^{-1/2} \sum_{i=1}^{N} w_i \exp(0.75\mu_{ij}^2)\, dX_j(t,\mu_{ij})/dt \qquad (14)$$

The performance of the present computers allows the application of high N values. We employed N=80 in our calculations. The reliability of the procedure were estimated by comparing the results at N=50 and N=80. In our calculations the relative precision of the Gauss - Hermite quadrature at N=80 proved to be better then 10^{-7} in this way. Here the following question arises: Why should one need such a high precision when the model itself is only approximate? The answer is: only a sufficiently good precision can ensure that all features of the calculated curves will reflect the properties of the model employed. Without the rescaling outlined above, we observed oscillations superposed on some of our simulated curves. It is known, however,

that such oscillations appear when the numerical solution of the DAEM employs an insufficient precision.[13,18]

Least squares curve fitting. The non-linear least squares method was employed. Denoting the observed data of the *k*th experiment and their simulated counterparts by $Y_k^{obs}(t)$ and $Y_k^{calc}(t)$, respectively, we minimize the following sum:

$$S = \sum_{k=1}^{N_{exp}} \sum_{i=1}^{N_k} [Y_k^{obs}(t_i) - Y_k^{calc}(t_i)]^2 / N_k / h_k^2 \qquad (15)$$

Here N_{exp} is the number of experimental curves evaluated simultaneously and N_k is the number of points on the *k*th evaluated curve. (N_k varied between 100 and 1000 in the calculations.) h_k denotes the height of *k*th evaluated curve:

$$h_k = \max Y_{ik}^{obs} \qquad (16)$$

The normalization by h_k proved to be useful to evaluate simultaneously experiments having strongly differing magnitudes[19,20]. As an example, we may consider that the heights of the DTG peaks in experiments 1 and 2 were 1.6×10^{-4} and 6.5×10^{-4} s^{-1}, respectively, due to the different heating rates employed. Without normalization by h_k, experiment 2 would have a ca. 16 times higher representation in the least squares sum than experiment 1.

Our algorithm searched for those parameters that minimized the least squares sum. Contrary to previous investigators[7-12], we did not fix the value of the pre-exponential factors. In this way, we had to determine a larger number of unknown parameters. This was accomplished by evaluating simultaneously experiments carried out at different kinds of temperature programs, as shown in Table 2 and Figure 1.

For each experimental curve, the obtained fit was characterized the following quantity:

$$fit\ (\%) = 100 \left(\sum_{i=1}^{N_k} [Y_{ik}^{obs} - Y_{ik}^{calc}]^2 / N_k \right)^{1/2} / h_k \qquad (17)$$

The temperature of the partial processes can be characterized by the temperature belonging to 50% conversion at a standardized heating rate, which was selected to be 10°C/min in the present work. These quantities, denoted by $T_{50\%,j}$, are tabulated together with the kinetic parameters.

The experimental data were processed by FORTAN 90 and C++ programs developed by the authors. More emphasis was placed on the reliability of the iterations than on the computational speed. The non-linear least squares parameters were determined by a direct search method.[16], which works reasonably on irregular surfaces, too. The results of the iterations were checked by restarting the searches with different

initial parameters. No statistical significance could be given to the obtained *fit* and parameter values, since the experimental errors of thermal analysis are neither random nor independent.[21]

Handling the c_j coefficients during the iteration. When a given mass spectrometric intensity did not exhibit overlapping peaks, there was no need to assume partial reactions, and only a c_1 coefficient arose for a given experimental curve. It was obtained in each iteration step by scaling the calculated dx_1/dt curve to the magnitude of observations by a least squares formula. In case of overlapping partial peaks, normalized $c_{j,norm}$ parameters were introduced:

$$c_{j,norm} = c_j / C_{sum}, \quad \text{where} \quad C_{sum} = \sum_{j=1}^{M} c_j \tag{18}$$

Since the sum of $c_{j,norm}$ is 1, these quantities characterize the ratios of the peak areas. We show here the procedure we employed in the case of M=2, where

$$c_{1,norm} = c_1 / (c_1+c_2) \quad \text{and} \quad c_{2,norm} = 1 - c_{1,norm} \tag{19}$$

We varied $c_{1,norm}$ together with the kinetic parameters during the nonlinear least squares evaluation. Whenever the non-linear optimization algorithm required the calculation of the least squares sum, a normalized function was formed from the simulated curves:

$$Y_{norm}(t) = c_{1,norm}\, dx_1/dt + (1 - c_{1,norm})\, dx_2/dt \tag{20}$$

This $Y_{norm}(t)$ function was scaled up to the magnitude of observations by a least squares formula to calculate $Y^{calc}(t)$ for equation (15). The scale factor obtained in this way equals to C_{sum}. (Cf. eqns. (2), (18) and (20).) The multiplication of $c_{1,norm}$ and $(1 - c_{1,norm})$ by C_{sum} provided c_1 and c_2. Similar method was employed at higher M, too.

As described in the Experimental section, the mass spectrometric intensities of ions CH_3^+, $C_xH_y^+$ and H_2^+ could not be calibrated. Accordingly, the corresponding c_j coefficients do not have a direct physical meaning. Among these curves, the intensity of H_2^+ exhibited overlapping peaks. Though the absolute amounts of the hydrogen formed in the peaks could not be determined, the relative amounts, expressed by the $c_{j,norm}$ coefficients were determined as described above and listed in the corresponding tables.

Results and discussion

Only those mass spectrometric curves were evaluated that had an abundance well above the noise level and base-line uncertainties. We shall discuss first the simple, single peak curves. The evaluation of the curves composed of overlapping partial curves is left to the end of the treatment.

CH_3^+. This fragment ion, *m/z* 15, is characteristic of methane, but also forms from virtually all compounds containing CH_3 groups. Consequently, it is produced in a relatively wide interval that ranges from 400 to 800 °C in the 10°C/min experiments. The corresponding peaks are well represented by the DAEM kinetics. There was no need to assume partial reactions in this case. The simultaneous evaluation of the six experiments resulted in E = 190 kJ/mol, σ = 17.5 kJ/mol and log A = 9.74. The question arises: how formal is this approximation? A simple way to check the reliability of a model is to study how suitable it is to predict phenomena outside the domain used in the determination of its parameters. For this reason, we repeated the evaluation with only two constant-heating rate measurements (experiments 1 and 2 in Table 2). This procedure resulted in similar kinetic parameters: E = 198 kJ/mol, σ = 18.4 kJ/mol and log A = 10.3. The differences between the parameter data set are not significant: a 4% change in E and the corresponding increase of log A is less than the usual uncertainties of non-isothermal kinetics with simple first order models.[21] Using these parameters we produced theoretical curves for all other experiments and obtained a reasonable fit as shown in Figure 2. It is particularly interesting to observe that the parameters obtained from constant-heating rate measurements describe well the isothermal sections, too.

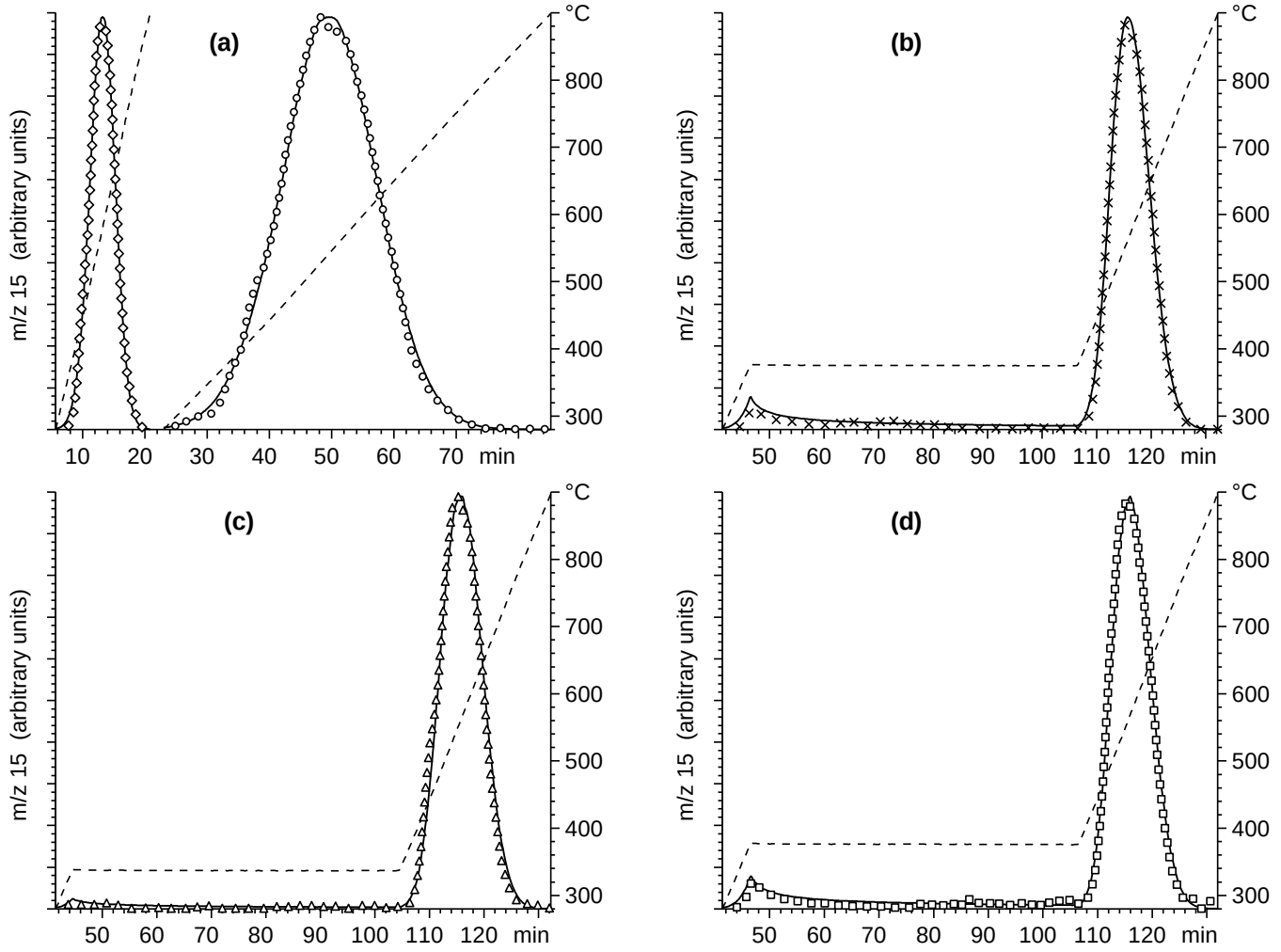

Figure 2: The kinetic parameters obtained from the CH_3^+ intensity curves of experiments 1 and 2 (panel a) are able to predict the experimental data at different heating programs of both the bottom (panel b) and the top reactor fractions (panels c, d). Symbols (o, ◊, ×, ∇, Δ, ρ): experimental curves. Solid line: simulated experimental curve. Dashed line: temperature program.

$C_xH_y^+$. From this family three ions were observed with sufficiently good signal/noise ratio: *m/z* 26 ($C_2H_2^+$), *m/z* 27 ($C_2H_3^+$), and *m/z* 29 ($C_2H_5^+$). They are characteristic of the decomposition of the aliphatic side groups in the char. The evaluation of their intensities in the six experiments resulted in activation energies of 167 – 184 kJ/mol, as indicated in Table 3. Ions with *m/z* 26 and 27 form in relatively narrow intervals ($\sigma \approx 10$ kJ/mol). The σ of *m/z* 29 is larger, 14.6 kJ/mol, which may be due to the fact that *m/z* 29 also involves CHO^+ ions formed from the decomposition of oxygenated groups.

Table 3: Results of the evaluation of curves CH_3^+, $C_2H_2^+$, $C_2H_3^+$, $C_2H_5^+$ (*m/z* 15, 26, 27 and 29)

Curve evaluated	E_0 (kJ/mol)	σ (kJ/mol)	log A (log s^{-1})	$T_{50\%}$ (°C) at 10°C/min
CH_3^+	190.0	17.5	9.74	538
$C_2H_2^+$	167.3	8.3	9.41	467
$C_2H_3^+$	184.0	10.2	10.73	461
$C_2H_5^+$	177.7	14.6	10.82	431

H_2^+. In this case we observed two partially overlapping peaks: a smaller one around 600°C and a larger one around 700-800°C. The smaller peak is more significant in the sample taken from the top fraction of the reactor, where the char, receiving less heat during preparation, has more volatiles. The smaller H_2^+ peak may be due to the aromatization of the biomass char, while the high temperature H_2 is evolved from the formation of larger polyaromatic structures during carbonization. The H_2^+ intensities of the six experiments were simultaneously evaluated, as shown in Figure 3. Keeping in mind that the top and bottom fraction samples had different compositions, we determined different $c_{j,norm}$ values for the top and for the bottom fractions, while the rest of the parameters were assumed to be identical. Table 4 shows the resulting parameters. The $c_{j,norm}$ values obtained for the top and the bottom fraction samples are listed in separate columns.

Table 4: Results of the evaluation of the H_2^+ curves (*m/z* 2)

j	$E_{0,j}$ (kJ/mol)	σ_j (kJ/mol)	log A_j (log s^{-1})	$c_{j,norm}$ bottom fr.	$c_{j,norm}$ top fr.	$T_{50\%,j}$ (°C) at 10°C/min
1	127	0.05	5.3	0.09	0.16	577
2	177	13.0	6.4	0.91	0.84	755

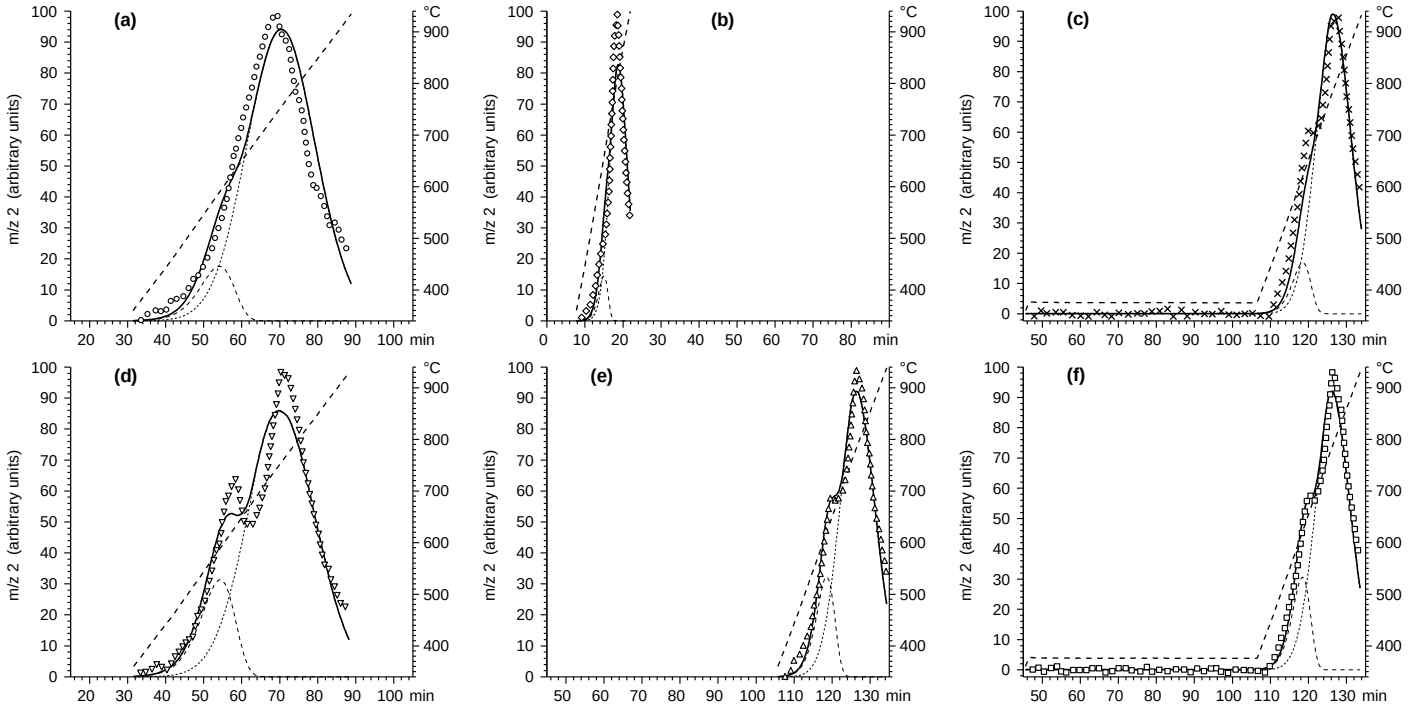

Figure 3: Simultaneous evaluation of the H_2^+ intensity curves of experiments 1 – 6 (Panels a – f). Symbols (o, ◊, ×, ∇, Δ, ρ): experimental curves. Bold solid line (**—**): simulated experimental curve. Thin lines of different styles (- - -, ····): simulated curves of the partial reactions. Bold dashed line (**– – –**): temperature program.

Oxygenated compounds. We were unable to obtain a reliable kinetic description for the mass spectrometric intensities associated with the evolution of H_2O, CO and CO_2. Their MS intensity curves were distorted by the following complicating factors: (i) these compounds react to each other via reversible reactions on the surfaces of the sample, the equipment walls and the deposited impurities (tars); (ii) the tar, depositing in the various parts of the equipment during an experiment reacts with the oxygen traces in the system and contribute to the H_2O, CO and CO_2 evolution at higher temperatures.

Overall mass loss rate curves. The DTG curves are formed by the merging of numerous elementary processes. Many partial curves may overlap each other, hence the DTG curves of the present work were well approximated by assuming only four partial peaks, as shown in Figure 4. The partial peaks, represented by thin lines of various line styles, can be best seen in the figures of the 10°C/min experiments, in panels (a) and (d). It is interesting to observe in panels (c), (e) and (f) that an isothermal section followed by a further heat-up split the partial peaks. This may be due to the characteristics of the distributed activation energy model employed. The lower side of the activation energy distribution represents the more reactive part of the corresponding chemical structures, which decomposes in the isothermal sections, while the less reactive species survive until the subsequent heating-up. The first peak, between room temperature and ca. 250°C, has $T_{50\%}$ = 177 °C, and corresponds to the loss of moisture during drying and the evaporation of organics trapped on the surface of the samples. The second peak, at $T_{50\%}$ = 418°C, describes the decomposition of side groups with low thermal stability (carboxyl, carbonyl, and aliphatic hydrocarbon groups.) The third peak at $T_{50\%}$ = 484°C represents the splitting-off of more resistant side groups and the formation of aromatic

rings. At higher temperatures, the aromatic compounds merge into larger units, releasing the excess hydrogen and their oxygen heteroatoms in the form of H_2O, CO, CO_2 and H_2.[14] These processes are described by the fourth peak of the model, at $T_{50\%}$ = 691°C. The corresponding kinetic parameters are listed in Table 5. The $c_{j,norm}$ values, characterizing the ratios of the peak areas, were obtained by a procedure similar to that of the previous section. We determined different sets of $c_{j,norm}$ values for the top and for the bottom fractions, while the kinetic parameters, A_j, $E_{0,j}$, *and* σ_j, were assumed to be identical. The c_j factors were calculated from the $c_{j,norm}$ values, as described in section Calculations. In the case of mass loss rate curves, the c_j factors give the amount of volatiles forming during a unit mass of sample in a given partial reaction. The top fraction charcoal releases a higher amount of volatiles, as it was discussed in our previous work.[14] The comparison of the bottom and top fraction c_j values in Table 5 show that the increased volatilization arises from the 2nd and 3rd partial reactions.

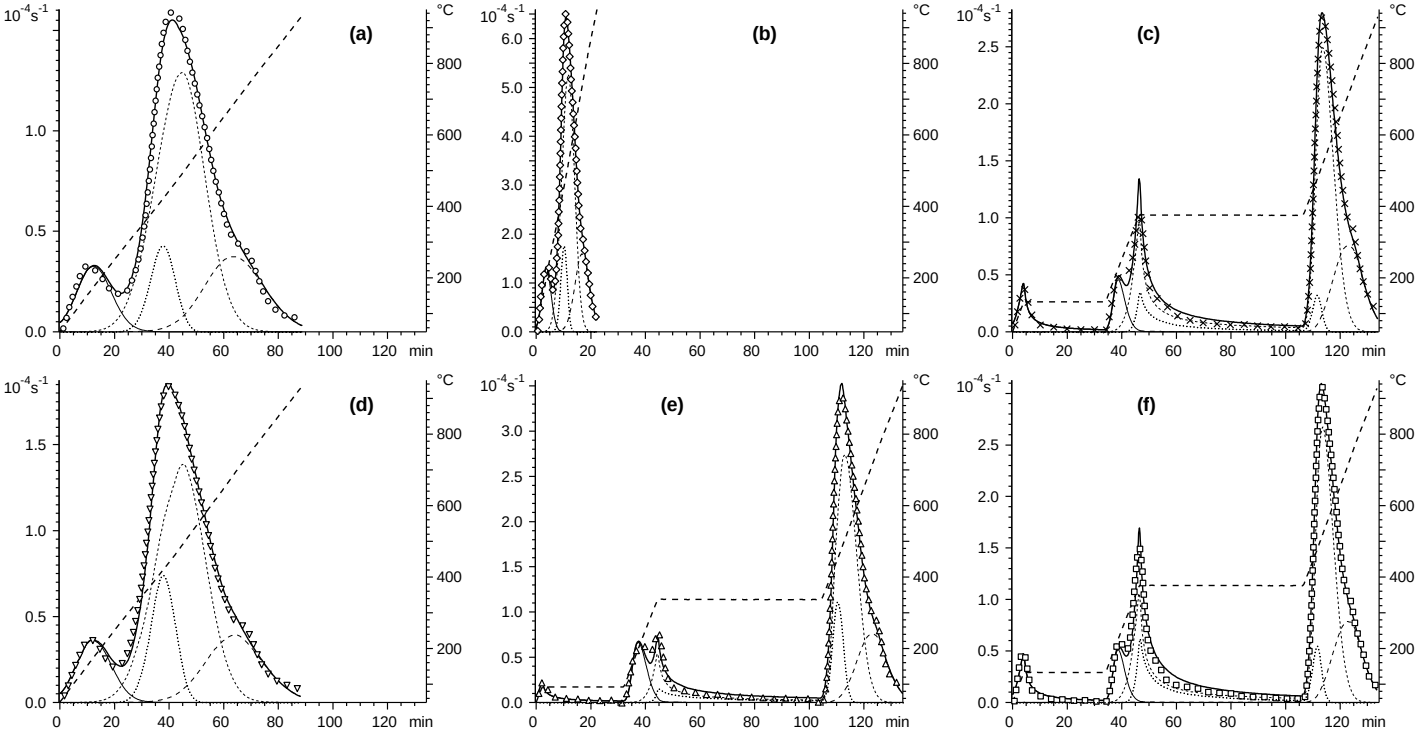

Figure 4: Simultaneous evaluation of the DTG curves of experiments 1 – 6 (Panels a – f). Symbols (o, ◊, ×, ∇, Δ, ρ): experimental curves. Bold solid line (**—**): simulated experimental curve. Thin lines of different styles (—, - - -, ····, ····): simulated curves of the partial reactions. Bold dashed line (**– – –**): temperature program.

Table 5: Results of the evaluation of the DTG curves (-dm/dt)

j	$E_{0,j}$ (Kj/mol)	σ_j (kJ/mol)	log A_j (log s^{-1})	$c_{j,norm}$ bottom fr.	$c_{j,norm}$ top fr.	c_j bottom fr.	c_j top fr.	$T_{50\%,j}$ (°C) at 10°C/min
1	87	12.2	7.9	0.11	0.10	0.03	0.03	177
2	181	9.6	11.4	0.10	0.15	0.03	0.05	418
3	211	25.1	12.2	0.59	0.56	0.18	0.19	484
4	229	25.4	9.9	0.21	0.19	0.06	0.06	691

Conclusion

1) DTG curves and mass spectrometric intensity curves often represent overlapping partial curves. The simultaneous evaluation of several experiments with different kinds of temperature programs enables a less ambiguous description of the overlapping curves by distributed activation energy models. There is no need to fix the pre-exponential factors in the model, since a properly chosen set of experiments can provide enough information to determine the unknown parameters.

2) The same DAEM equations with the same parameters described equally well the non-isothermal experiments and the experiments containing isothermal sections of a given sample.

3) The mass spectrometric ion intensities associated with the evolution of methane and aliphatic hydrocarbons were well described by the conventional single distributed activation energy reaction model. The model proved to be capable of predicting the behavior of the samples under experimental conditions differing from the ones used for the determination of the kinetic parameters.

4) Hydrogen evolution was described by two, parallel, distributed activation energy reactions. The smaller H_2^+ peak may result from the aromatization of the biomass char, while the high temperature H_2 is evolved during the formation of the larger polyaromatic structures during carbonization.

5) The description of the overall mass loss curve (DTG) required four, parallel, distributed activation energy reactions. The first peak, at $T_{50\%}$ = 177°C, corresponded to the drying and the evaporation of the organics trapped on the surface of the samples. The second peak, at $T_{50\%}$ = 418°C, described the decomposition of the side groups with low thermal stability (carboxyl, carbonyl, and aliphatic hydrocarbon groups.) The third peak, at $T_{50\%}$ = 484°C, represented the splitting-off of the more resistant side groups and the formation of the aromatic rings. The last peak, at $T_{50\%}$ = 691°C, described the decomposition of the heat resistant heteroaromatic structures and the formation of polyaromatic structures. The charcoal taken from the top fraction of the reactor released more volatiles in the second and third partial reactions.

Acknowledgment

Research conducted in Hungary was supported by the Hungarian National Research Fund (OTKA T025347 and T025341). Research conducted in Hawaii was supported by the National Science Foundation (Grant CTS95-21423), and the Coral Industries Endowment of the University of Hawaii.

Nomenclature

A_j = pre-exponential factor of the rate constant (s^{-1})

c_j = coefficients to form linear combinations from the calculated $-dx_j/dt$ functions

$c_{j,norm}$ = c_j parameters normalized so that their sum would be unity

C_{sum} = sum of the c_j coefficients

$D_j(E)$ = normalized distribution function

E_j = activation energy (kJ mol^{-1})

$E_{0,j}$ = parameter of Gaussian distribution (kJ mol^{-1})

h_k = the height of kth evaluated curve

$m(t)$ = mass of the sample divided by the initial sample mass

M = number of partial reactions contributing to a given measured quantity

N_{exp} = number of experimental curves evaluated simultaneously

N_k = number of evaluated data for the kth experimental curve

R = gas constant (8.3143×10^{-3} kJ mol^{-1} K^{-1})

S = least squares sum

t = time (s)

T = temperature (K)

$T_{50\%}$ = temperature belonging to 50% conversion at a constant heating rate of 10°C/min

$x_j(t)$ = unreacted fraction of a given species in the jth kinetic equation. ($x_j(0) = 1$, $x_j(\infty) = 0$.)

$X_j(E,t)$ = solution of a 1st order kinetic equation at a given activation energy value E. ($X_j(0,E) = 1$, $X_j(\infty,E) = 0$.)

$Y^{obs}(t)$ and $Y^{calc}(t)$ = an experimental curve and its simulated counterpart

w_i = weight factors of the Guass – Hemite quadrature formula

$\varepsilon_j = 2\,(E-E_{0,j})/\sqrt{2}\,\sigma_j$

$\mu_j = 2\,(E-E_{0,j})/\sqrt{2}\,\sigma_j$

σ_j = parameter of Gaussian distribution (kJ mol^{-1})

References

(1) Antal, M. J.; Croiset, E., Dai, X.; DeAlmeida, C.; Mok, W. S. L.; Norberg, N.; Richard, J. R.; Mamoun, A. M. High-yield biomass charcoal. *Energy Fuels* **1996**, 10, 652-658.

(2) Antal, M. J., Jr. Process for charcoal production from woody and herbaceous plant material. U.S.A. Patent 5,435,983, 1995.

(3) Antal, M. J.; Allen, S. G.; Dai, X.; Shimizu, B.; Tam, M. S.; Grønli, M. G. Attainment of the theoretical yield of carbon from biomass. *Ind. Eng. Chem. Res.* **2000,** *39*, 4024-4031.

(4) Wenzl, H. F. J. *The Chemical Technology of Wood*; Acadamic Press, New York, 1970.

(5) Antal, M.J.; Dai, X.; Shimizu, B.; Tam, M.S.; Grønli, M. New prospects for biocarbons. In *Progress in Thermochemical Biomass Conversion*; A.V. Bridgwater, ed., Blackwell Science, Oxford, England, 2001, pp. 1179-1185.

(6) Burnham, A. K.; Braun, R.L. Global kinetic analysis of complex materials. *Energy Fuels* **1999**, 13, 1-22.

(7) Anthony, D. B.; Howard, J. B. Coal devolatilization and hydrogasification. *AICHE J*, **1976**, *22*, 625-656.

(8) Solomon, P. R.; Hamblen, D.G.; Serio, M. A.; Yu, Z.Z.; Charpenay, S. A characterization method and model for predicting coal conversion behavior. *Fuel* **1993**, *72*, 469-488.

(9) Agarwal, P.K. Distributed kinetic-parameters for methane evolution during coal pyrolysis. *Fuel* **1985**, *64*, 870-872.

(10) Heidenreich, C. A.; Yan, H. M.; Zhanga, D. K. Mathematical modelling of pyrolysis of large coal particles—estimation of kinetic parameters for methane evolution. *Fuel*, **1999**, *78*, 557-566.

(11) Agarwal, P.K.; Agnew, J.B.; Ravindran, N.; Weimann, R. Distributed kinetic-parameters for the evolution of gaseous species in the pyrolysis of coal. *Fuel*, **1987**, 66, 1097-1106.

(12) Lázaro, M. J.; Moliner, R.; Suelves, I. Non-isothermal versus isothermal technique to evaluate kinetic parameters of coal pyrolysis. *J. Anal. Appl. Pyrolysis* **1998**, *47*, 111-125.

(13) Donskoi, E.; McElwain, D. L. S. Optimization of coal pyrolysis modeling. *Combustion Flame* **2000**, *122*, 359-367

(14) Várhegyi, G.; Szabó, P.; Till, F.; Zelei, B.; Antal, M. J., Jr.; Dai, X. TG, TG-MS, and FTIR characterization of high-yield biomass charcoals. *Energy Fuels* **1998**, *12*, 969-974.

(15) Várhegyi, G.; Antal, M. J., Jr.; Székely, T.; Till, F.; Jakab, E. Simultaneous thermogravimetric - mass spectrometric studies on the thermal decomposition of biopolymers. Part 1: Avicel cellulose in the presence and absence of catalysts. *Energy Fuels* **1988**, *2*, 267-272.

(16) W. H. Press, B. P. Flannery, S. A. Teukolsky, W. T. Vetterling, *Numerical Recipes. The Art of Scientific Computing*; Cambridge University Press, Cambridge (U.K.), 1986.

(17) Visual Numerics, Inc. *IMSL Fortran 90 Mathematical Programming Library, Version 3.0*; IMSL Software, Houston, TX USA 1996.

(18) Günes, S; Günes M. The influences of various parameters on the numerical solution of nonisothermal DAEM equation. *Thermochim. Acta* **1999**, *336*, 93-96.

(19) Várhegyi, G.; Szabó, P.; Mok W. S. L., Antal, M. J., Jr. Kinetics of the thermal decomposition of cellulose in sealed vessels at elevated pressures. Effects of the presence of water on the reaction mechanism. *J. Anal. Appl. Pyrolysis*, **1993,** *26*, 159-174.

(20) Conesa, J. A.; Marcilla, A.; Font, R.; Caballero, J.A. Thermogravimetric studies on the thermal decomposition of polyethylene. *J. Anal. Appl. Pyrolysis*, **1996**, *36*, 1-15.

(21) Grønli, M.; Antal, M. J., Jr.; Várhegyi, G., A round-robin study of cellulose pyrolysis kinetics by thermogravimetry. *Ind. Eng. Chem. Res*. **1999,** *38*, 2238-2244.